LETTER

doi:10.1038/nature14579

A very luminous magnetar-powered supernova associated with an ultra-long γ-ray burst

Jochen Greiner[1,2], Paolo A. Mazzali[3,4], D. Alexander Kann[1,2,5], Thomas Krühler[6], Elena Pian[7,8], Simon Prentice[3], Felipe Olivares E.[9], Andrea Rossi[5,7], Sylvio Klose[5], Stefan Taubenberger[4,10], Fabian Knust[1], Paulo M. J. Afonso[11], Chris Ashall[3], Jan Bolmer[1,12], Corentin Delvaux[1], Roland Diehl[1], Jonathan Elliott[1,13], Robert Filgas[14], Johan P. U. Fynbo[15], John F. Graham[1], Ana Nicuesa Guelbenzu[5], Shiho Kobayashi[3], Giorgos Leloudas[15,16], Sandra Savaglio[1,17], Patricia Schady[1], Sebastian Schmidl[5], Tassilo Schweyer[1,12], Vladimir Sudilovsky[1,13], Mohit Tanga[1], Adria C. Updike[18], Hendrik van Eerten[1] & Karla Varela[1]

A new class of ultra-long-duration (more than 10,000 seconds) γ-ray bursts has recently been suggested[1–3]. They may originate in the explosion of stars with much larger radii than those producing normal long-duration γ-ray bursts[3,4] or in the tidal disruption of a star[3]. No clear supernova has yet been associated with an ultra-long-duration γ-ray burst. Here we report that a supernova (SN 2011kl) was associated with the ultra-long-duration γ-ray burst GRB 111209A, at a redshift *z* of 0.677. This supernova is more than three times more luminous than type Ic supernovae associated with long-duration γ-ray bursts[5–7], and its spectrum is distinctly different. The slope of the continuum resembles those of super-luminous supernovae[8,9], but extends further down into the rest-frame ultraviolet implying a low metal content. The light curve evolves much more rapidly than those of super-luminous supernovae. This combination of high luminosity and low metal-line opacity cannot be reconciled with typical type Ic supernovae, but can be reproduced by a model where extra energy is injected by a strongly magnetized neutron star (a magnetar), which has also been proposed as the explanation for super-luminous supernovae[10].

GRB 111209A was detected by the Swift satellite at 07:12 UT on 9 December 2011. The X-ray and optical counterparts were discovered within minutes[11]. The extraordinarily long duration of GRB 111209A was revealed by the continuous coverage provided by the Konus detector on the WIND spacecraft[12], extending from ~5,400 s before to ~10,000 s after the Swift trigger. The GRB occurred at a redshift of $z = 0.677$, as determined from afterglow spectroscopy[3]. Its integrated equivalent isotropic energy output, $E_{iso} = (5.7 \pm 0.7) \times 10^{53}$ erg (ref. 12), lies at the bright end of the distribution of long-duration GRBs.

The afterglow of GRB 111209A was observed over a period of about 70 days with the seven-channel optical/near-infrared imager GROND[13]. Starting around day 15, the optical light curve deviated from the earlier afterglow power-law decay (Fig. 1). The light curve remained essentially flat between days 15 and 30, and then started to decay again, approaching the host-galaxy level. After subtracting the afterglow and the well-modelled host galaxy emission (Methods, first three sections), the excess emission is well constrained between rest-frame days (that is, observed days divided by $(1 + z)$) 6 and 43 after the GRB (Fig. 2). This excess emission (Table 1) is very similar in shape to other GRB-related supernovae, but reaches a bolometric peak luminosity of $2.8^{+1.2}_{-1.0} \times 10^{43}$ erg s^{-1} (corresponding to a bolometric magnitude $M_{bol} = -20.0$ mag) at 14 rest-frame days, a factor of three times higher than the brightest known GRB-associated supernova (Fig. 2).

A spectrum was taken with the X-shooter instrument on the Very Large Telescope (ESO) near the peak of the excess emission[3] (29 December 2011), 11.8 rest-frame days after the GRB. The afterglow and the (minimal) host contribution were subtracted (Methods section 'The host galaxy') and the resulting spectrum is shown in Fig. 3 (blue line). The strong similarity of the evolution in time and colour to GRB-associated supernovae, together with the spectral shape of the excess emission, leads us to conclude that this emission is caused by a supernova, designated SN 2011kl, associated with GRB 111209A.

Canonical long-duration GRBs are generally accepted to be linked to the core collapse of massive stars stripped of their outer H and He envelopes[5–7], since every spectroscopically confirmed supernova associated with a GRB has been a broad-lined type Ic so far. Although the spectrum of SN 2011kl associated with the ultra-long GRB 111209A also shows no H or He, it is substantially different from classical GRB-associated supernovae. It is surprisingly featureless on the long-wavelength side ('redwards') of 300 nm, lacking the undulations from spectral line blends typical of broad-lined type Ic supernovae associated with GRBs[5–7], and it does not drop in the 300–400 nm (rest-frame) region (Fig. 3), suggesting a very low metal abundance. Applying standard parametrized supernova light-curve fits (Methods section 'Radioactivity cannot power the supernova peak'), we derive an ejecta mass $M_{ej} = 3 \pm 1\ M_{\odot}$ and a ^{56}Ni mass of $1.0 \pm 0.1\ M_{\odot}$, which implies a very high ^{56}Ni/M_{ej} ratio ($M_{\odot}$, solar mass). This large ^{56}Ni mass is not compatible with the spectrum, suggesting that ^{56}Ni is not responsible for the luminosity, unlike canonical stripped-envelope supernovae (Methods section 'Radioactivity cannot power the supernova peak').

Various models have been suggested to explain the ultra-long duration of GRB 111209A and other ultra-long GRBs, but the otherwise inconspicuous spectral and timing properties of both the prompt and afterglow emission as well as the host properties provided no obvious clues[1–4,14–16]. With the detection of a supernova associated with the ultra-long GRB 111209A, we can immediately discard a tidal disruption interpretation[3]. Known supernovae from blue supergiants show hydrogen in their spectra and substantially different light-curve

[1]Max-Planck-Institut für Extraterrestrische Physik, Giessenbachstrasse 1, 85748 Garching, Germany. [2]Excellence Cluster Universe, Technische Universität München, Boltzmannstrasse 2, 85748 Garching, Germany. [3]Astrophysics Research Institute, Liverpool John Moores University, IC2, Liverpool Science Park, 146 Browlow Hill, Liverpool L3 5RF, UK. [4]Max-Planck-Institut für Astrophysik, Karl-Schwarzschild-Strasse 1, 85748 Garching, Germany. [5]Thüringer Landessternwarte Tautenburg, Sternwarte 5, 07778 Tautenburg, Germany. [6]European Southern Observatory, Alonso de Córdova 3107, Vitacura, Casilla 19001, Santiago 19, Chile. [7]INAF, Institute of Space Astrophysics and Cosmic Physics, via P. Gobetti 101, 40129 Bologna, Italy. [8]Scuola Normale Superiore, Piazza dei Cavalieri 7, I-56126 Pisa, Italy. [9]Departamento de Ciencias Fisicas, Universidad Andres Bello, Avenida Republica 252, Santiago, Chile. [10]European Southern Observatory, Karl-Schwarzschild-Strasse 2, 85748 Garching, Germany. [11]American River College, Physics and Astronomy Department, 4700 College Oak Drive, Sacramento, California 95841, USA. [12]Technische Universität München, Physik Department, James-Franck-Strasse, 85748 Garching, Germany. [13]Astrophysics Data System, Harvard–Smithonian Center for Astrophysics, Garden Street 60, Cambridge, Massachusetts 02138, USA. [14]Institute of Experimental and Applied Physics, Czech Technical University in Prague, Horska 3a/22, 128 00 Prague 2, Czech Republic. [15]DARK Cosmology Center, Niels-Bohr-Institut, University of Copenhagen, Juliane Maries Vej 30, 2100 København, Denmark. [16]Department of Particle Physics and Astrophysics, Weizmann Institute of Science, Rehovot 76100, Israel. [17]Universita della Calabria, 87036 Arcavacata di Rende, via P. Bucci, Italy. [18]Roger Williams University, 1 Old Ferry Road, Bristol, Rhode Island 02809, USA.

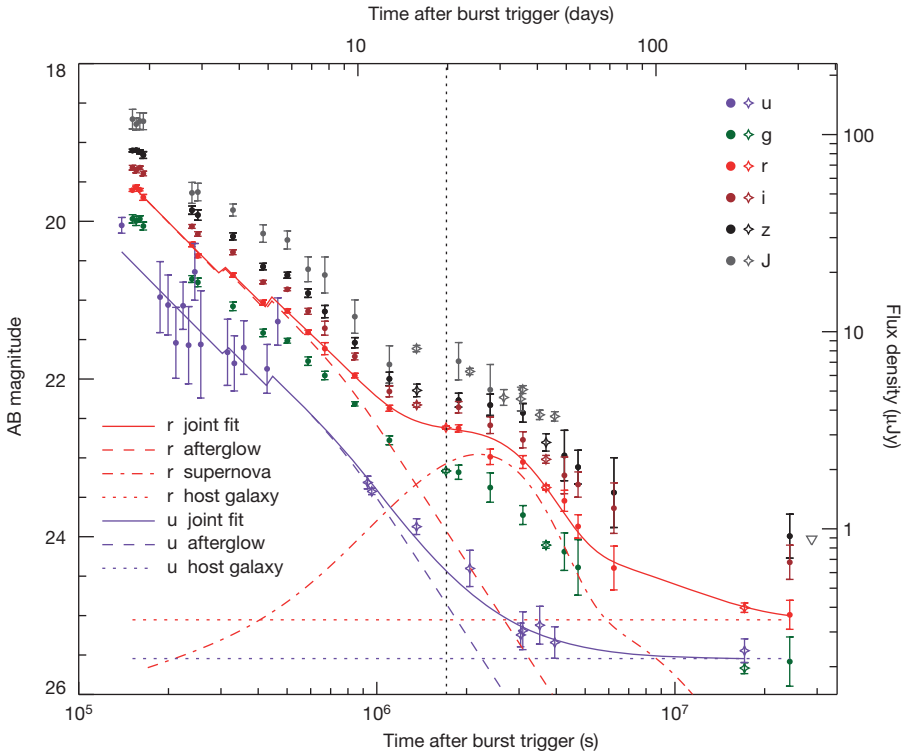

Figure 1 | Observed optical/near-infrared light curve of GRB 111209A. Data points (GROND data, filled symbols; other data, open symbols) show measured magnitudes. The fitted light curve (solid red line) is the sum of the afterglow of GRB 111209A modelled by a broken power law (dashed red line), the accompanying supernova SN 2011kl (dash-dotted red line) and the constant host galaxy emission (horizontal dotted red line). The u′-band data are well fitted without a supernova component, that is, the sum of only the afterglow and host (solid violet line). All measurements (error bars, 1σ uncertainty) are relative to the Swift trigger time and as observed, apart from the Vega-to-AB transformation for the J band. The vertical dotted line marks the time of the VLT/X-shooter spectrum.

properties[17], inconsistent with our observations, thus ruling out a blue supergiant progenitor[4]. Finally, additional emission from the interaction of the supernova ejecta with circumstellar material is also unlikely (Methods section 'Enhanced emission due to interaction with the circumburst medium?').

Our data suggest that SN 2011kl is intermediate between canonical overluminous GRB-associated supernovae and super-luminous supernovae (Fig. 3). The latter are a sub-class of supernovae that are a factor of ~100 brighter than normal core-collapse supernovae, reaching a V-band magnitude $M_V \approx -21$ mag (refs 8, 9). They show slow rise times and late peak times (peak times about 20–100 days as compared to typically 9–18 days). Their spectra are characterized by a blue continuum with a distinctive "W"-shaped spectral feature often interpreted as O II lines[8]. A spinning-down magnetic neutron star is the favoured explanation for the energy input powering the light curve[10]. The comparison of SN 2011kl with super-luminous

Table 1 | AB magnitudes of SN 2011kl associated with GRB 111209A

Δt (s)	g′ mag	r′ mag	i′ mag	z′ mag	J mag
843, 664	$24.36^{+0.26}_{-0.21}$	$23.92^{+0.23}_{-0.19}$	$24.03^{+0.55}_{-0.38}$	$23.97^{+1.13}_{-0.57}$	
1,101,930	$24.17^{+0.29}_{-0.24}$	$23.66^{+0.16}_{-0.14}$	$23.80^{+0.44}_{-0.33}$	$23.83^{+0.75}_{-0.48}$	
1,358,649					22.38 ± 0.09
1,360,463			$23.28^{+0.12}_{-0.11}$		
1,361,742				$23.16^{+0.28}_{-0.25}$	
1,705,078	23.59 ± 0.04				
1,706,253		22.99 ± 0.04			
1,880,549	23.47 ± 0.15	22.90 ± 0.07	22.74 ± 0.13	$22.78^{+0.19}_{-0.18}$	$22.18^{+0.39}_{-0.35}$
2,049,952					22.30 ± 0.06
2,401,323	$23.53^{+0.28}_{-0.27}$	23.25 ± 0.15	22.90 ± 0.17	$22.67^{+0.23}_{-0.22}$	$22.54^{+0.53}_{-0.48}$
2,664,187					$22.62^{+0.16}_{-0.15}$
3,037,306					$22.58^{+0.22}_{-0.21}$
3,085,966					22.41 ± 0.07
3,090,966	$23.88^{+0.18}_{-0.17}$	23.21 ± 0.11	$23.05^{+0.17}_{-0.16}$	22.70 ± 0.19	
3,518,554					22.81 ± 0.09
3,692,304			23.35 ± 0.12		
3,693,574				$23.21^{+0.23}_{-0.22}$	
3,694,905	24.36 ± 0.07				
3,696,071		23.60 ± 0.05			
3,950,847					22.81 ± 0.09
4,258,444	$24.41^{+0.39}_{-0.37}$	23.80 ± 0.20	$23.63^{+0.42}_{-0.40}$	$23.44^{+0.62}_{-0.58}$	
4,732,196	$24.69^{+0.63}_{-0.58}$	$24.28^{+0.27}_{-0.26}$	$23.80^{+0.32}_{-0.31}$	$23.67^{+0.48}_{-0.46}$	
6,241,880		$25.26^{+0.84}_{-0.74}$	$24.29^{+0.78}_{-0.73}$	$24.27^{+1.57}_{-1.34}$	

The data are corrected for the GRB afterglow and host-galaxy contributions, as well as Galactic foreground and rest-frame extinction. Errors are at the 1σ confidence level and include error propagation from the afterglow and host subtraction. The first column (Δt) is the time after the GRB in the observer frame. The magnitudes without contemporaneous g′, r′, i′, z′ magnitudes are taken from ref. 3.

supernovae is motivated by two observational facts: (1) the spectrum is a blue continuum, extending far into the rest-frame ultraviolet, and (2) the peak luminosity is intermediate between GRB-associated supernovae and super-luminous supernovae. Our interpretation is motivated by the failure of both the collapsar and the standard fall-back accretion scenarios, because in these cases the engine quickly runs out of mass for any reasonable accretion rate and mass reservoir, and thus is unlikely to be able to power an ultra-long GRB.

We could reproduce the spectrum of SN 2011kl using a radiation transport code[18,19] and a radial (r) density (ρ) profile where $\rho \propto r^{-7}$, which is typical of the outer layers of supernova explosions. The ultraviolet emission is significantly depressed relative to a blackbody, but much less depressed than in the spectra of GRB-associated supernovae, indicating a lower metal content (consistent with 1/4 of the solar metallicity). The spectrum appears rather featureless owing to line blending. This follows from the high photospheric velocity, $v_{ph} \approx 20{,}000$ km s^{-1} (Fig. 3). In contrast, super-luminous supernovae, which show more line features, have $v_{ph} \approx 10{,}000$ km s^{-1}. In the optical part of the spectrum, on the other hand, only a few very weak absorption lines are visible in our supernova spectrum. Our model only has $\sim$0.4 $M_\odot$ of material above the photosphere. There is no evidence of freshly synthesized material mixed-in, unlike the case of GRB-associated supernovae. This supports the notion that the supernova light curve was not powered by Ni decay but rather by a magnetar.

The supernova spectrum can be reproduced without invoking interaction, and the low metal abundance suggests that it is unlikely that much Ni was produced. We therefore consider magneto-rotational energy input as the source of luminosity. Using a simple formalism[20] describing rotational energy loss via magnetic dipole radiation, and relating the spin-down rate to the effective radiative diffusion time, we can infer the magnetar's initial spin period, P_i, and magnetic dipole field strength, B, from the observed luminosity and time to light-curve peak, t_{peak}. The observed short t_{peak} ($\sim$14 rest-frame days) and the moderate peak luminosity require a magnetar with initial spin period $P_i \approx 12$ ms for a magnetic field strength of (6–9) $\times$ 10^{14} G. Depending on the magnetic field that is assumed, calculated values of ejecta mass and kinetic energy are relatively uncertain, ranging between 2 and 3 $M_\odot$ and (2–9) $\times$ 10^{51} erg, respectively (Methods section 'Modelling'). These values are actually more typical of normal type Ib/c supernovae than of GRB-associated supernovae, including SN 2006aj, the first supernova identified as magnetar-powered[21]. The GRB energy can be reconciled with the maximum energy that can be extracted from a magnetar if the correction for collimation of the GRB jet is a factor of 1/50 or less, which is well within typical values for GRBs[22].

The idea of a magnetar as the inner engine powering GRB-associated supernovae[23,24], super-luminous supernovae[10], or even events like Swift 1644+57[25] (before consensus for this event favoured a relativistic tidal disruption), is not new. However, in all these cases the magnetar interpretation was one of several options providing reasonable fits to the data, never the only option. Also, the suggestion that all GRB-associated supernovae are magnetars[24] rather than collapsars, based on the clustering of the kinetic energy of the GRB-associated supernovae near 10^{52} erg, the rotational power of a millisecond neutron star, was only circumstantial evidence for the magnetar origin. The supernova SN 2011kl is clearly different from canonical GRB-associated supernovae, and requires (rather than only allows) a new explanation.

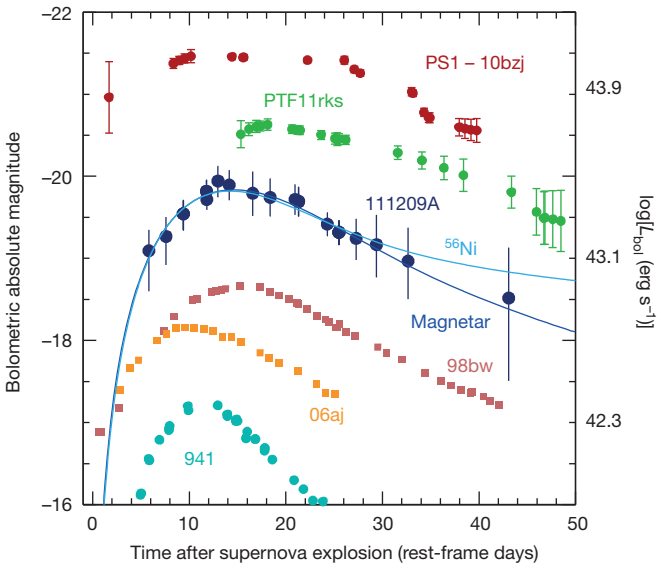

Figure 2 | Light curve of the supernova (SN 2011kl) linked with GRB 111209A and of other objects. Shown is the bolometric light curve of SN 2011kl, corresponding to 230–800 nm rest frame wavelengths (Methods section 'Observations and data analysis'), compared with those of GRB 980425/SN 1998bw[5], XRF 060218/SN 2006aj[21], the standard type Ic SN 1994I[26], and the super-luminous supernovae PTF11rks[27] and PS1-10bzj[28] (among the fastest-declining super-luminous supernovae known so far), all integrated over the same wavelength band with 1σ error bars. Solid lines show the best-fitting synthetic light curves computed with a magnetar injection model[20] (dark blue; Methods section 'Modelling') and ^{56}Ni powering (light blue; Methods section 'Radioactivity cannot power the supernova peak').

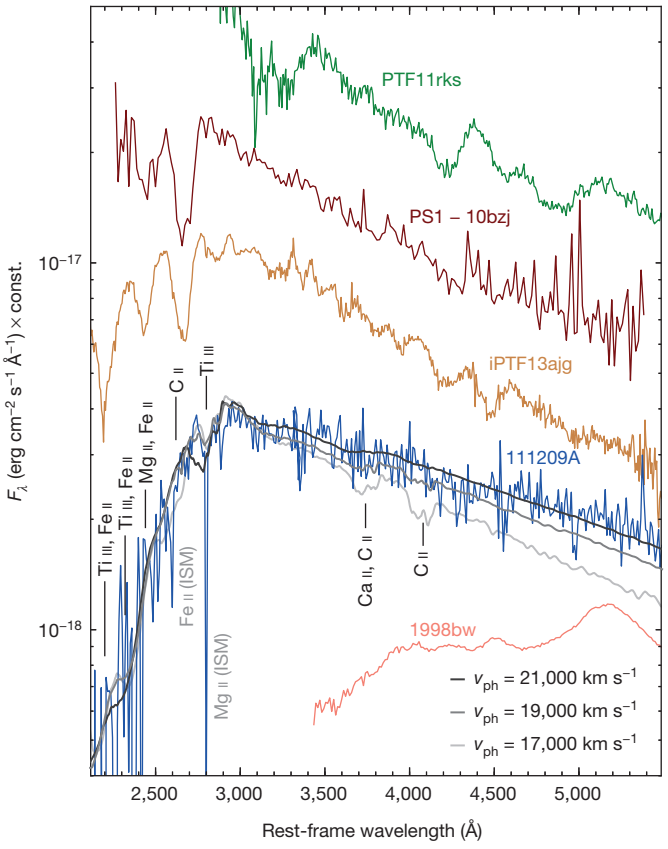

Figure 3 | Spectra comparison. The X-shooter spectrum of SN 2011kl, associated with GRB 111209A, taken on 29 December 2011 after GRB afterglow and host subtraction and moderate rebinning (Methods section 'Observations and data analysis'; Extended Data Fig. 2), with its flat shape and high ultraviolet flux, is distinctly different from the hitherto brightest known GRB-associated supernova 1998bw (red), but reminiscent of some super-luminous supernovae (top three curves)[28–30]. The three grey/black lines show synthetic spectra with different photospheric velocities (as labelled), demonstrating the minimum velocity required to broaden unseen absorption around 400 nm rest-frame (Ca II, C II), but at the same time explain the sharp cut-off below 280 nm rest-frame. The y scale is correct for SN 2011kl and SN 1998bw; all other spectra are shifted for display purposes.

The ultra-long duration of the prompt emission of GRB 111209A and the unusual supernova properties are probably related. We suggest that they are linked to the birth and subsequent action of a magnetar following the collapse of a massive star. The magnetar re-energizes the expanding ejecta and powers an over-luminous supernova. This particular supernova, SN 2011kl, was not quite as luminous as typical super-luminous supernovae, and it may represent a population of events that is not easily discovered by supernova searches but which may occur at a relatively high rate. This scenario offers a link between GRB-associated supernovae, ultra-long GRBs and super-luminous supernovae.

Online Content Methods, along with any additional Extended Data display items and Source Data, are available in the online version of the paper; references unique to these sections appear only in the online paper.

Received 10 December 2014; accepted 8 May 2015.

1. Gendre, B. *et al.* The ultra-long gamma-ray burst 111209A: the collapse of a blue supergiant? *Astrophys. J.* **766,** 30 (2013).
2. Stratta, G. *et al.* The ultra-long gamma-ray burst 111209A: II. Prompt to afterglow and afterglow properties. *Astrophys. J.* **779,** 66 (2013).
3. Levan, A. *et al.* A new population of ultra-long duration gamma-ray bursts. *Astrophys. J.* **781,** 13 (2014).
4. Nakauchi, D., Kashiyama, K., Suwa, Y. & Nakamura, T. Blue supergiant model for ultra-long gamma-ray bursts with superluminous-supernova-like bump. *Astrophys. J.* **778,** 67 (2013).
5. Galama, T. *et al.* An unusual supernova in the error box of the γ-ray burst of 25 April 1998. *Nature* **395,** 670–672 (1998).
6. Hjorth, J. *et al.* A very energetic supernova associated with the γ-ray burst of 29 March 2003. *Nature* **423,** 847–850 (2003).
7. Stanek, K. Z. *et al.* Spectroscopic discovery of the supernova 2003dh associated with GRB 030329. *Astrophys. J.* **591,** L17–L20 (2003).
8. Quimby, R. M. *et al.* Hydrogen-poor superluminous stellar explosions. *Nature* **474,** 487–489 (2011).
9. Gal-Yam, A. Luminous supernovae. *Science* **337,** 927–932 (2012).
10. Dessart, L., Hillier, D. J., Waldman, R., Livne, E. & Blondin, S. Superluminous supernovae: Ni power versus magnetar radiation. *Mon. Not. R. Astron. Soc.* **426,** L76–L80 (2012).
11. Hoversten, E. A. *et al.* GRB 111209A: Swift detection of a long burst with an optical counterpart. *GCN Circ.* **12632** (2011).
12. Golenetskii, S. *et al.* Konus-Wind observation of GRB 111209A. *GCN Circ.* **12663** (2011).
13. Greiner, J. *et al.* GROND — a 7-channel imager. *Publ. Astron. Soc. Pacif.* **120,** 405–424 (2008).
14. Virgili, F. J. *et al.* GRB 091024A and the nature of ultra-long gamma-ray bursts. *Astrophys. J.* **778,** 54 (2013).
15. Zhang, B.-B., Zhang, B., Murase, K., Connaughton, V. & Briggs, M. S. How long does a burst burst? *Astrophys. J.* **787,** 66 (2014).
16. Leloudas, G. *et al.* Spectroscopy of superluminous supernova host galaxies. A preference of hydrogen-poor events for extreme emission line galaxies. *Mon. Not. R. Astron. Soc.* **449,** 917–932 (2015).
17. Kleiser, I. K. W. *et al.* Peculiar Type II supernovae from blue supergiants. *Mon. Not. R. Astron. Soc.* **415,** 372–382 (2011).
18. Mazzali, P. A. & Lucy, L. B. The application of Monte Carlo methods to the synthesis of early-time supernovae spectra. *Astron. Astrophys.* **279,** 447–456 (1993).
19. Mazzali, P. A. Applications of an improved Monte Carlo code to the synthesis of early-time supernova spectra. *Astron. Astrophys.* **363,** 705–716 (2000).
20. Kasen, D. & Bildsten, L. Supernova light curves powered by young magnetars. *Astrophys. J.* **717,** 245–249 (2010).
21. Mazzali, P. A. *et al.* A neutron-star-driven X-ray flash associated with supernova SN 2006aj. *Nature* **442,** 1018–1020 (2006).
22. Ryan, G., van Eerten, H., MacFadyen, A. & Zhang, B.-B. Gamma-ray bursts are observed off-axis. *Astrophys. J.* **799,** A3 (2015).
23. Cano, Z. A trio of gamma-ray burst supernovae: GRB 120729A, GRB 130215A/SN 2013ez, and GRB 130831A/SN 2013fu. *Astron. Astrophys.* **568,** 19 (2014).
24. Mazzali, P. A. *et al.* An upper limit to the energy of gamma-ray bursts indicates that GRBs/SNe are powered by magnetars. *Mon. Not. R. Astron. Soc.* **443,** 67–71 (2014).
25. Quataert, E. & Kasen, D. Swift 1644+57: the longest gamma-ray burst? *Mon. Not. R. Astron. Soc.* **419,** L1–L5 (2012).
26. Sauer, D. N. *et al.* The properties of the 'standard' type Ic supernova 1994I from spectral models. *Mon. Not. R. Astron. Soc.* **369,** 1939–1948 (2006).
27. Inserra, C. Super-luminous Type Ic supernovae: catching a magnetar by the tail. *Astrophys. J.* **770,** 128 (2013).
28. Lunnan, R. *et al.* PS1–10bzj: a fast, hydrogen-poor superluminous supernova in a metal-poor host galaxy. *Astrophys. J.* **771,** 97 (2013).
29. Vreeswijk, P. M. *et al.* The hydrogen-poor superluminous supernova iPTF 13ajg and its host galaxy in absorption and emission. *Astrophys. J.* **797,** 24 (2014).
30. Yaron, O. & Gal-Yam, A. WISeREP — an interactive supernova data repository. *Publ. Astron. Soc. Pacif.* **124,** 668–681 (2012).

Acknowledgements We thank R. Lunnan and E. Berger for providing the spectrum of PS1-10bzj in digital form, and A. Levan for the HST grism spectra of GRB 111209A. J.G., R.D. and D.A.K. acknowledge support by the DFG cluster of excellence "Origin and Structure of the Universe" (http://www.universe-cluster.de). P.S., J.F.G. and M.T. acknowledge support through the Sofja Kovalevskaja award to P.S. from the Alexander von Humboldt Foundation, Germany. C.D. acknowledges support through EXTraS, funded from the European Union's Seventh Framework Programme for research, technological development and demonstration. S.K., D.A.K. and A.N.G. acknowledge support by DFG. S. Schmidl acknowledges support by the Thüringer Ministerium für Bildung, Wissenschaft und Kultur. F.O.E. acknowledges support from FONDECYT. S.T. is supported by DFG. R.F. acknowledges support by Czech MEYS. Part of the funding for GROND (both hardware as well as personnel) was generously granted from the Leibniz-Prize to G. Hasinger. DARK is funded by the DNRF.

Author Contributions J.G. led the observing campaign and the paper writing. D.A.K. was responsible for the GROND data reduction, and performed the fitting of the afterglow light curve. F.K. derived the accurate GROND astrometry, P.S. the UVOT photometry, and A.R. the host fitting. P.M. suggested the magnetar interpretation and computed the spectral models. S.P. and C.A. performed the light-curve model fitting. F.O.E. and E.P. assisted in spectral decomposition and the construction of the bolometric light curve. S.T., S.K. and G.L. provided crucial input and discussion. D.A.K., A.N.G., P.M.J.A., J.B., C.D., J.E., R.F., J.F.G., S. Schmidl, T.S., V.S., M.T., A.C.U. and K.V. performed the many epochs of GROND observations. T.K., J.P.U.F. and G.L. provided and analysed the X-shooter spectrum. S. Savaglio, S.K., R.D. and H.v.E. were instrumental in various aspects of the data interpretation.

Author Information Reprints and permissions information is available at www.nature.com/reprints. The authors declare no competing financial interests. Readers are welcome to comment on the online version of the paper. Correspondence and requests for materials should be addressed to J.G. (jcg@mpe.mpg.de).

METHODS

Observations and data analysis. Simultaneous imaging in g′, r′, i′, z′, J, H, K_s with the 7-channel imager GROND[13] was done on 16 epochs with logarithmic temporal spacing until 72 days after the GRB, when the nearby Sun prevented further observations, and a last epoch for host photometry was obtained 280 days after the GRB (Extended Data Table 1). GROND data have been reduced in the standard manner using pyraf/IRAF[31–33]. The optical imaging was calibrated against comparison stars obtained by observing a nearby SDSS field (immediately before the afterglow observation in the third night under photometric conditions) and calibrated against the primary SDSS[34] standard star network. The near-infrared data were calibrated against the 2MASS catalogue. This results in typical absolute accuracies of ±0.03 mag in g′, r′, i′, z′, and ±0.05 mag in J, H, K_S (1σ errors are reported everywhere). All GROND measurements are listed in Extended Data Table 1, and the properties of the GRB afterglow proper, including the two kinks in the early afterglow light curve (Fig. 1) will be described in detail elsewhere (D.A.K. *et al.*, manuscript in preparation).

We have made use of two other sources of measurements: First, we add u-band observations obtained with Swift/UVOT (Extended Data Table 2). UVOT photometry was carried out on pipeline-processed sky images downloaded from the Swift data centre[35] following the standard UVOT procedure[36], and is fully compatible with earlier, independent publications of the UVOT data[2,3]. Second, we add selected complementary data[3], in particular (i) HST F336W/F125W data from 11.1 and 35.1 days after the GRB, respectively; (ii) two epochs of VLT/FORS2 g′, R_C, i′, z′, data during the supernova phase, which agree excellently with our data due to their use of our GROND calibration stars; (iii) a late-time Gemini-S u′-band observation (198 days after the GRB).

With the constant host galaxy contribution accurately determined at late times in u′, g′, r′, i′, z′, J (see Methods section 'The host galaxy' and Extended Data Fig. 4), the afterglow light curve shows clear evidence for a steeper afterglow decay at >10 days post-burst, particularly in the u′-band where there is essentially no contribution from the supernova (as evidenced by the spectrum) and which therefore can be used as a template for the pure afterglow contribution. We link the decay slopes for all filters to each other, so we use the same single fit parameter for all filters. This provides the two decay slopes $\alpha_1 = 1.55 \pm 0.01$ and $\alpha_2 = 2.33 \pm 0.16$, with a break time of $t_b = 9.12 \pm 0.47$ days. The u′-band fit is also shown in Fig. 1 to visualize the decomposition. Apart from our much larger data set provided by our GROND observations, the difference between our fit and the decomposition of ref. 3 is the fact that in the latter the host contribution in the redder bands at ~30−50 days was ignored (although this is noted in ref. 3).

In order to create the supernova light curve for each photometric band, we then subtracted both the afterglow contribution in that band based on the extrapolation of the afterglow light curve, and the host galaxy contribution based on its spectral energy distribution; see Methods section 'The host galaxy'). The error in the host galaxy subtraction is negligible as the host photometry is accurate to better than 10%, and the host contributes only 5–15% to the total light during the supernova bump. The error on the afterglow subtraction depends on whether or not the decay slope remained constant after the last secure measurement right before the onset of the supernova. The intrinsic GRB afterglow light curves at this late time are observed to only steepen, never flatten. Thus, our afterglow subtraction is conservative, and results in a lower limit for the supernova luminosity.

The quasi-bolometric light curve of SN 2011kl was constructed from GROND g′, r′, i′, z′, J photometry and the supplementary data from ref. 3 as follows. First, the individual filter bands have been extinction-corrected with $A_V^{Gal} = 0.06$ mag Galactic foreground[37], and rest-frame $A_V^{Host} = 0.12$ mag as derived from the GRB afterglow spectral energy distribution fitting. By deriving quadratic polynomials for sets of three consecutive filters (Simpson's rule), they were then combined to create a quasi-bolometric light curve.

The quadratic polynomials are then integrated over rest-frame wavelength from 3,860/(1 + z) Å (blue edge of the g′-band filter) to 13,560/(1 + z) Å (red edge of the J filter). The k-correction was computed from the spectral energy distribution. In order to transform the integrated flux into luminosity, we employed a luminosity distance of d = 4,080 Mpc, using concordance cosmology ($\Omega_\Lambda = 0.73$, $\Omega_m = 0.27$, and $H_0 = 71$ km s^{-1} Mpc^{-1}).

No correction for the contribution of the unobserved near-infrared part of the spectrum has been applied to SN 2011kl or SN 1998bw (Fig. 2), because this emission is usually sparsely sampled in wavelength and time, and thus is largely based on assumptions (and no data are available for the plotted super-luminous supernovae). For SN 2011kl we lack any rest-frame near-infrared measurements. We acknowledge that therefore the bolometric luminosity might be underestimated by 5–30%. Other than that, all bolometric light curves shown in Fig. 2 are integrated over the same wavelength band (except for the ultraviolet band, which contributes less than a few percent at and after maximum). The super-luminous supernovae light curves are plotted according to the observational constraints of their maxima, that is, g-band peak at 16.8 days rest-frame for PTF11rks[27] and using the first measurement 17.5 days before maximum as lower limit for PS1-10bzj[28].

The VLT/X-shooter[38] spectrum, taken on 29 December 2011 (19.8 days after the GRB, 11.8 rest-frame days, and 2 days before the supernova maximum), has been reduced with the ESO X-shooter pipeline v2.2.0, in particular for flat-fielding, order tracing, rectification and initial wavelength calibration with an arc lamp. During rectification, a dispersion of 0.4 Å per pixel has been used in the UVB/VIS arm, minimizing correlated noise but maintaining sufficient spectral resolution for resolving lines down to ~50 km s^{-1}, that is, a velocity dispersion of 20 km s^{-1}. Our own software is used for bad-pixel and cosmic-ray rejection, as well as sky-subtraction and frame shifting and adding[39]. Optimal extraction is applied to the resulting two-dimensional frames, and the one-dimensional spectrum is finally flux calibrated separately for each arm against the GROND photometry. Spectral binning has no effect on the steepness of the slope (Extended Data Fig. 1). The NIR arm does not contain any useful signal, nor do the two HST grism spectra[3] (Extended Data Fig. 2).

The observed spectrum is the sum of light from the GRB afterglow, the GRB host galaxy, and the supernova SN 2011kl. After correcting for $A_V^{Gal} = 0.06$ mag Galactic foreground[37] extinction, we corrected for the contribution of the host galaxy using a template fit (Methods section 'The host galaxy') on the host photometry (including the J-band measurement of ref. 3), and subtracted the afterglow based on the extrapolation of the g′, r′, i′, z′ GROND light curves to the time of the X-shooter observation. After conversion to the rest-frame, we corrected for intrinsic reddening of $E(B-V) = 0.04 \pm 0.01$ mag derived from the GROND afterglow SED fitting (see Extended Data Fig. 3 for the effect of each of these steps).

Association of GRB afterglow, supernova, and host galaxy. We detect narrow absorption lines of Mg II(λ2796, λ2803), Mg I(λ2852) and Fe II(λ2344, λ2374, λ2382, λ2586, λ2600) in the SN 2011kl spectrum. No change in equivalent widths and redshift is apparent when compared to the afterglow spectrum[3,39] taken 0.75 days after the GRB. Moreover, these equivalent widths are typical of those seen from host galaxies of bright long-duration GRBs. This relates the supernova to the same host galaxy as GRB 111209A.

No offset is measurable in GROND images between GRB afterglow and supernova (δRA < 0.032 arcsec, δDec. < 0.019 arcsec), which implies that the two events are co-spatial within <200 pc.

The host galaxy. During the late-epoch GROND observation the host galaxy is clearly detected in g′, r′, i′, z′ in the 3−5σ range (last entry in Extended Data Table 1). We add HST F336W and Gemini from ref. 3. Noting that the supernova does not contribute significantly any more during these late epochs (with expected AB magnitudes g′ ≈ 28.5, r′ ≈ 28.0, i′ ≈ 27.5, z′ ≈ 27.2 mag), we employ LePHARE[40] and use the best-fit model (a low-mass, star-forming galaxy) as a template for the host subtraction (see Extended Data Figs 3 and 4). Inferences on the physical properties of the host from this fitting will be published elsewhere (D.A.K. *et al.*, manuscript in preparation) and absorption/emission line information from the optical/near-infrared X-shooter spectra are given in ref. 39. We note though that the low metal content seen in the supernova spectrum is in accord with the very low host galaxy metallicity (10–40%), which is somewhat unusual for such a low-redshift object but commonly seen in super-luminous supernova hosts.

Radioactivity cannot power the supernova peak. Modelling the bolometric light curve according to the standard scheme of ^{56}Ni powering[41] and augmented by Co decay[42], an ejecta mass of 3.2 ± 0.5 $M_\odot$ and a ^{56}Ni mass of 1.0 ± 0.1 $M_\odot$ are derived (we used v_{ph} = 20,000 km s^{-1}, and a grey opacity of 0.07 ± 0.01 cm^2 g^{-1}, constant in time). The derived ^{56}Ni mass is anomalously large for type Ib/c supernovae, including GRB-associated supernovae[43]. Such a large ^{56}Ni mass is difficult to reconcile with the very low opacity in the blue part of the spectrum. The continuum flux keeps rising down to 300 nm rest-frame without any sign of suppression implying very low metal line opacity. Also, the ejected mass of ~3 $M_\odot$ as deduced from the light curve width is not consistent with the large ^{56}Ni mass.

While it has been suggested that part of the ^{56}Ni could be synthesized in the accretion disk[44], this is unlikely to proceed at the rate needed in our case. Recent numerical simulations show that for a wide range of progenitor masses (13–40 $M_\odot$), initial surface rotational velocities, metallicities and explosion energies, the required disk mass of more than 1 $M_\odot$ (corresponding to ~0.2 $M_\odot$ ^{56}Ni) is difficult to achieve[45], for both cases of compact objects: (i) in the case of heavy fallback, leading to the collapse of the central object into a black hole, the explosion energy is required to be small (few × 10^{48} erg), and more importantly, the disk forms only after a few months due to the large fallback time (~10^6 s); (ii) in the case of little fallback, leaving a neutron star behind, only fine-tuned conditions produce fallback disks at all, and these then have lifetimes of at most several hundred seconds.

Thus, a different mechanism must power the supernova light curve during the first ~40 days (rest frame).

Enhanced emission due to interaction with the circumburst medium?. Given the large luminosity, we considered additional emission from the interaction of the supernova ejecta with the circumstellar medium as an alternative possibility. In that case, one may expect narrow Balmer emission lines. While we detect very narrow ($\sigma = 35$ km s^{-1}) Hα, Hβ and [O III] lines in emission, the Balmer fluxes are compatible with the forbidden line flux and with an origin from the global low ($0.02\ M_\odot$ yr^{-1}) star formation rate in this low-metallicity (10–40% solar) host galaxy[39]. On the other hand, if the progenitor star was heavily stripped, no circumstellar H may be present. Another, more serious constraint is the very blue supernova spectrum, which would require a very low density to minimize extinction (though dust may be destroyed by the initial GRB and supernova light). This may be at odds with the requirement that the density is high enough to generate the few 10^{43} erg s^{-1} of radiative luminosity observed around the peak.

Modelling. We have been able to reproduce the spectrum of SN 2011kl using a radiation transport code[18,19] and a radial (r) density (ρ) profile where $\rho \propto r^{-7}$, which is typical of the outer layers of supernova explosions. The spectra appear rather featureless but this does not mean that there is no absorption: the ultraviolet is significantly depressed relative to a blackbody. However, it is much less depressed than in the spectra of GRB-associated supernovae, indicating a lower metal content. Many metal lines are active in the ultraviolet (Fe, Co, Ti, Cr). The smooth appearance of the ultraviolet spectrum is the result of the blending of hundreds of lines caused by the large range of wavelengths over which lines are active (line blanketing). Indeed, the photospheric velocity (and density) determines the degree of line blending. We used here photospheric velocities of $v_{\rm ph} \approx$ 20,000 km s^{-1} (grey/black lines in Fig. 3), and can see increasingly featureless spectra as $v_{\rm ph}$ increases and lines are active at higher velocities (larger blueshift), demonstrating the minimum velocity required to broaden unseen absorption around 400 nm rest-frame (Ca II, C II) and at the same time explain the sharp cut-off below 280 nm rest-frame. The strongest lines that shape this strong blue cut-off are labelled in black (grey 'ISM' labels mark Mg II/Fe II absorption lines in the host galaxy). Most of these are blended and do not stand out as individual features, unlike in classical super-luminous supernovae which have $v_{\rm ph} \approx 10{,}000$ km s^{-1}. In the optical, on the other hand, only a few very weak absorption lines are visible in our supernova spectrum. These are due to Ca II and C II lines. O II lines are not detected, and would require large departures from thermal equilibrium because of the very high ionization/excitation potential of their lower levels (20–30 eV). This suggests the presence of X-rays in super-luminous supernovae, probably produced by shocks. Our model only has ~0.4 $M_\odot$ of material above the photosphere. The metal content is quite low. It is consistent with 1/4 of the solar metallicity, which could be the metallicity of the star whose explosion caused the GRB and the supernova, and there is no evidence of freshly synthesized material mixed-in, unlike in GRB-associated supernovae. This supports the notion that the supernova light curve was not powered by Ni decay but rather by a magnetar. Figure 3 shows this model with three different photospheric velocities overplotted on the X-shooter spectrum.

The spectrum can be reproduced without invoking interaction, but the metal abundance is so low that it is unlikely that much ^{56}Ni has been produced. We therefore consider magneto-rotational energy input as the source of luminosity. Depending on the relative strength of magnetar and radioactive decay energy deposition, different peak luminosities as well as rise and decay times can be obtained[20]. One particularly pleasant feature of the magnetar mechanism is that it does not necessarily suffer from strong line blanketing, thus providing a more natural explanation for the observed spectrum.

Using a simple formalism describing rotational energy loss via magnetic dipole radiation and relating the spin-down rate to the effective radiative diffusion time, one can infer the magnetar's initial spin period $P_{\rm i}$ and magnetic dipole field strength from the observed luminosity and time to light curve peak $t_{\rm peak}$. One million combinations of the parameters $P_{\rm i}$, B, $M_{\rm ej}$ and $E_{\rm K}$ were sampled and ranked according to the goodness of fit relative to the data. All best solutions cluster at $P_{\rm i} = 12.2 \pm 0.3$ ms and have $B = (7.5 \pm 1.5) \times 10^{14}$ G, required by the observed short $t_{\rm peak}$ (~14 rest-frame days) and the moderate (for a magnetar) peak luminosity. Under the assumption that the magnetar is the sole contributor to the kinetic energy and to the light curve, a larger energy would be required from the magnetar, leading to $P_{\rm i} \approx 3$ ms and $B \approx 4 \times 10^{14}$ G. The mass and energy of the ejecta are less well determined, as they depend on the energy injection by the magnetar, and also due to the unknown distribution of mass in velocity space below the photosphere. We find a rather low ejected mass $M_{\rm ej} = 2.4 \pm 0.7\ M_\odot$, and energy $E_{\rm K} = (5.5 \pm 3.3) \times 10^{51}$ erg. Different photospheric velocities of, for example, 10,000, 15,000 and 20,000 km s^{-1} lead to different ejecta masses of 1.1, 1.7 and 2.2 $M_\odot$, but produce indistinguishable light curves with $M_{\rm Ni} = 1.1 \pm 0.1\ M_\odot$. Note though that not every combination of $P_{\rm i}$, $M_{\rm ej}$ and $E_{\rm K}$ yields similar results. The GRB energy can be reconciled with the maximum energy that can be extracted from a magnetar if the correction for collimation of the GRB jet is a factor of 1/50 or less, which is well within typical values for GRBs[22].

Code availability. The code used in refs 18, 19 is available on request from mazzali@mpa-garching.mpg.de.

31. Tody, D. in *Astronomical Data Analysis Software and Systems II* (eds Hanisch, R. J., Brissenden, R. J. V. & Barnes, J.) 173 (ASP Conf. Ser. 52, 1993).
32. Krühler, T. *et al.* The 2175 Å feature in a gamma-ray burst afterglow at redshift 2.45. *Astrophys. J.* **685,** 376–383 (2008).
33. Küpcü Yoldaş, A. *et al.* First results of GROND. *AIP Conf. Proc.* **1 000,** 227–231 (2008).
34. SDSS. http://www.sdss.org/dr3/algorithms/fluxcal.html (accessed 21 October 2014).
35. Swift: catching gamma-ray bursts on the fly. http://www.swift.ac.uk/swift_portal (2014).
36. Poole, T. S. *et al.* Photometric calibration of the Swift ultraviolet/optical telescope. *Mon. Not. R. Astron. Soc.* **383,** 627–645 (2008).
37. Schlegel, D., Finkbeiner, D. & Davis, M. Maps of dust infrared emission for use in estimation of reddening and cosmic microwave background radiation foregrounds. *Astrophys. J.* **500,** 525–553 (1998).
38. Vernet, J. *et al.* X-shooter, the new wide band intermediate resolution spectrograph at the ESO Very Large Telescope. *Astron. Astrophys.* **536,** A105 (2011).
39. Krühler, T. *et al.* GRB hosts through cosmic time: an emission-line survey of 96 gamma-ray burst selected galaxies between $0.1 < z < 3.6$. *Astron. Astrophys.* (in the press); preprint at http://arXiv.org/abs/1505.06743 (2015).
40. Arnouts, S. & Ilbert, O. Le PHARE: Photometric analysis for redshift estimate. http://www.cfht.hawaii.edu/~arnouts/LEPHARE (2014).
41. Arnett, W. D. Type I supernovae. I — Analytic solutions for the early part of the light curve. *Astrophys. J.* **253,** 785–797 (1982).
42. Valenti, S. *et al.* The broad-lined Type Ic supernova 2003jd. *Mon. Not. R. Astron. Soc.* **383,** 1485–1500 (2008).
43. Mazzali, P. A. *et al.* The very energetic, broad-lined Type Ic supernova 2010ah (PTF10bzf) in the context of GRB/SNe. *Mon. Not. R. Astron. Soc.* **432,** 2463–2473 (2013).
44. Surman, R., McLaughlin, G. C. & Hix, W. R. Nucleosynthesis in the outflow from gamma-ray burst accretion disks. *Astrophys. J.* **643,** 1057–1064 (2006).
45. Perna, R., Duffell, P., Cantiello, M. & MacFadyen, A. I. The fate of fallback matter around newly born compact objects. *Astrophys. J.* **781,** 119 (2014).
46. Cardelli, J. A., Clayton, G. C. & Mathis, J. S. The relationship between infrared, optical, and ultraviolet extinction. *Astrophys. J.* **345,** 245–256 (1989).

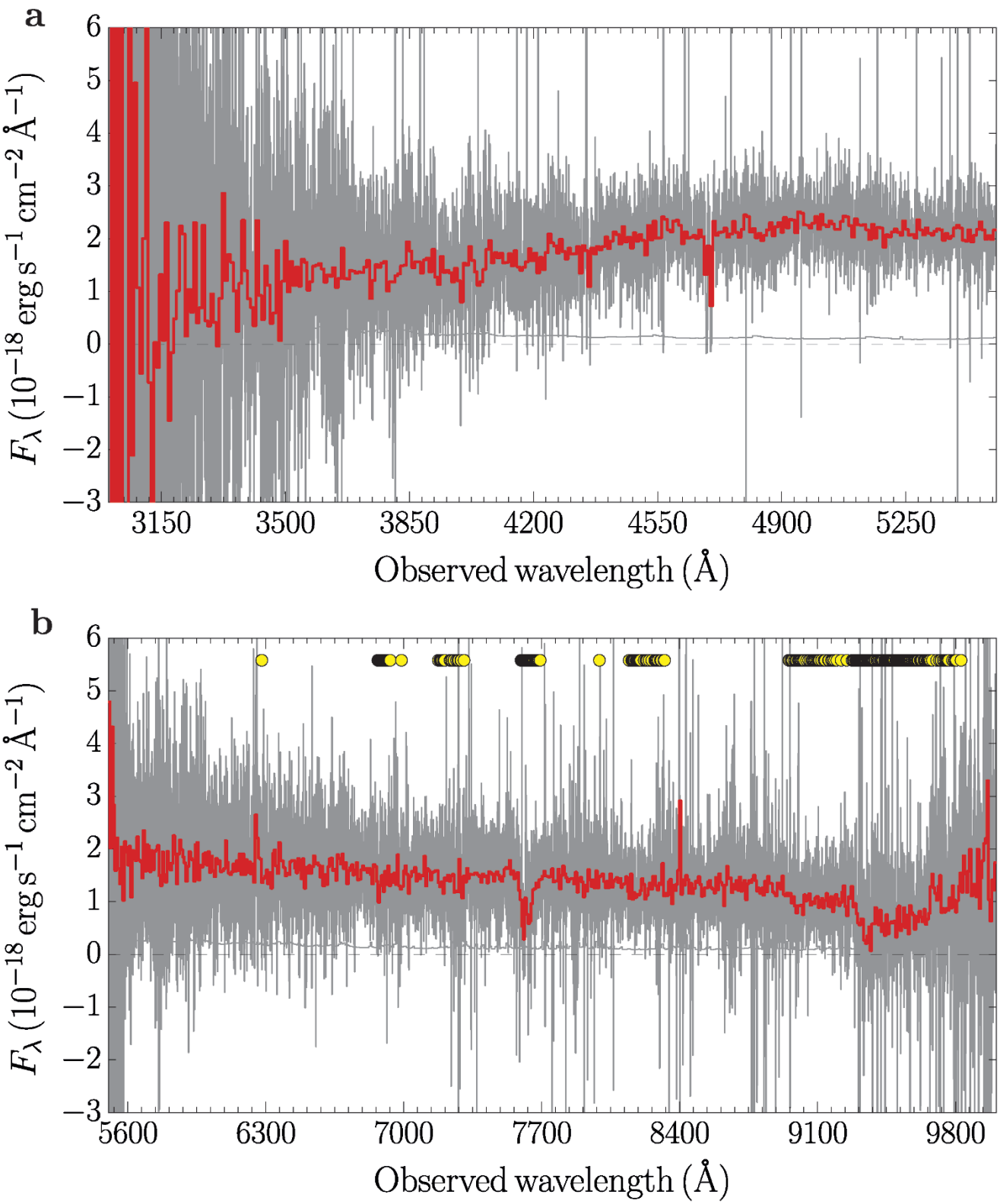

Extended Data Figure 1 | Binning has no effect on spectral slope. Original X-shooter spectrum in the UVB (**a**) and VIS (**b**) arms shown in grey (0.4 Å per pixel; before host and afterglow subtraction), with the re-binned (factor of 20) spectrum overplotted in black. The binning does not change the steepness of the spectrum, in particular not at the blue end. Yellow circles denote positions of atmospheric absorption lines.

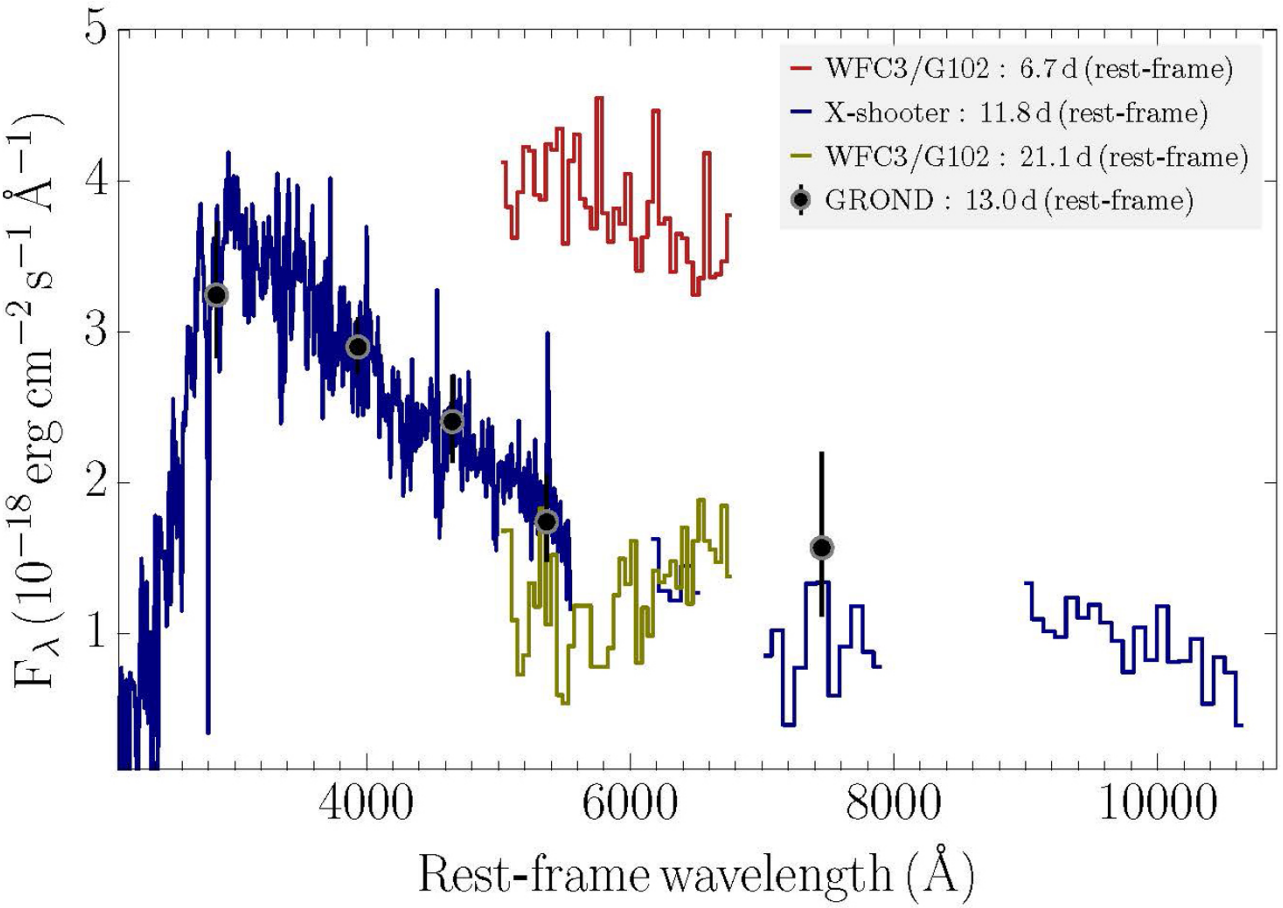

Extended Data Figure 2 | Long-wavelength spectra. Full X-shooter spectrum near maximum light of SN 2011kl, as well as two HST grism spectra taken one week before and after the supernova maximum (both taken from ref. 3). Above 500 nm rest-frame, none contain any informative absorption lines (all absorption structures seen are from the Earth's atmosphere).

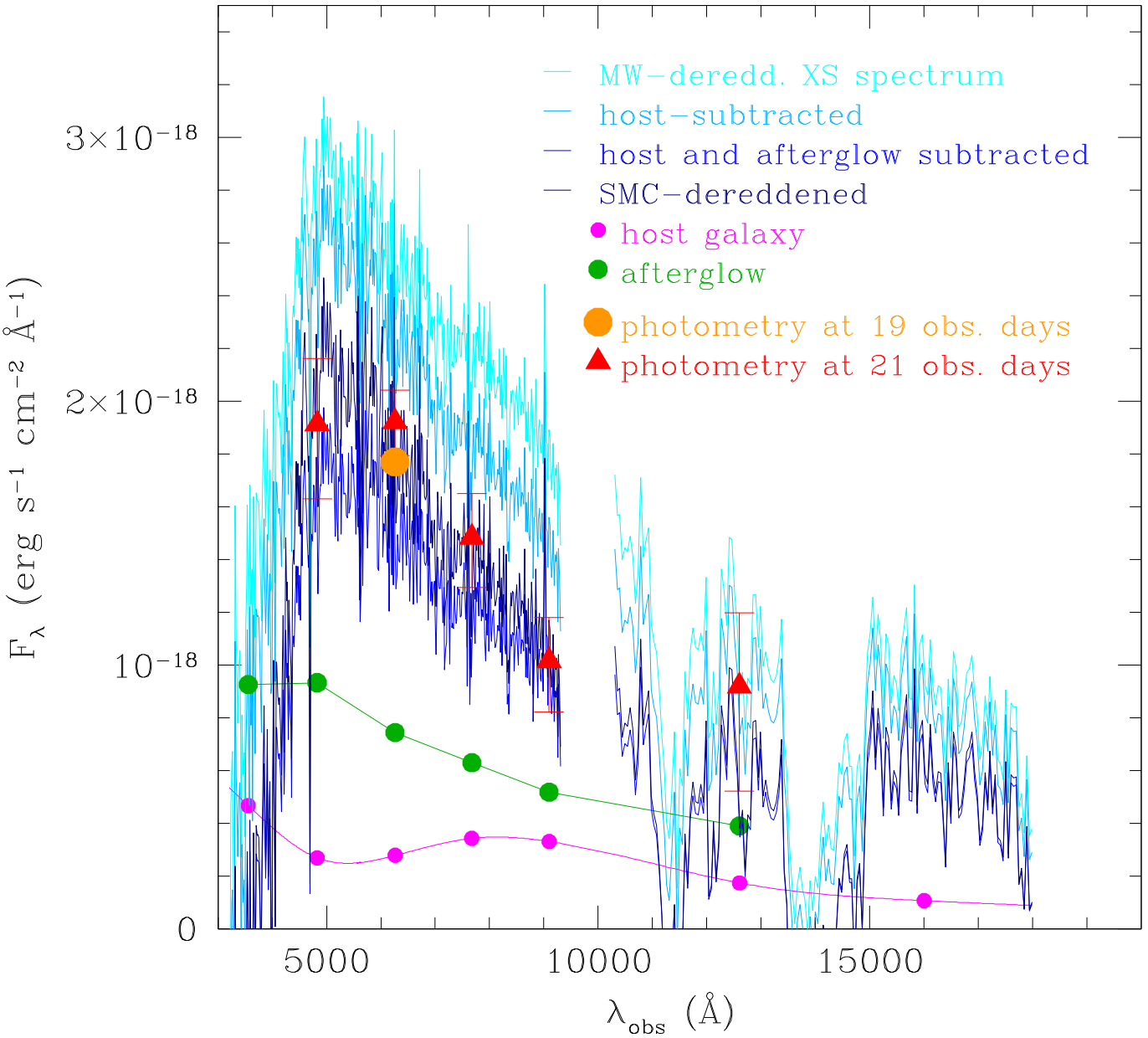

Extended Data Figure 3 | Step-by-step corrections of the supernova spectrum. Sequence of analysis steps for the X-shooter spectrum; from the observed spectrum corrected only for galactic foreground (top, very light blue), through host subtraction (light blue) and afterglow+host subtraction (blue) to local host (SMC-like) dereddened (very dark blue). The break at 500 nm observer-frame (300 nm rest-frame) and the steep slope towards the ultraviolet are inherent to the raw spectrum, not a result of afterglow or host subtraction. The coloured data points are the photometric observations in the individual UVOT+GROND+Gemini filters.

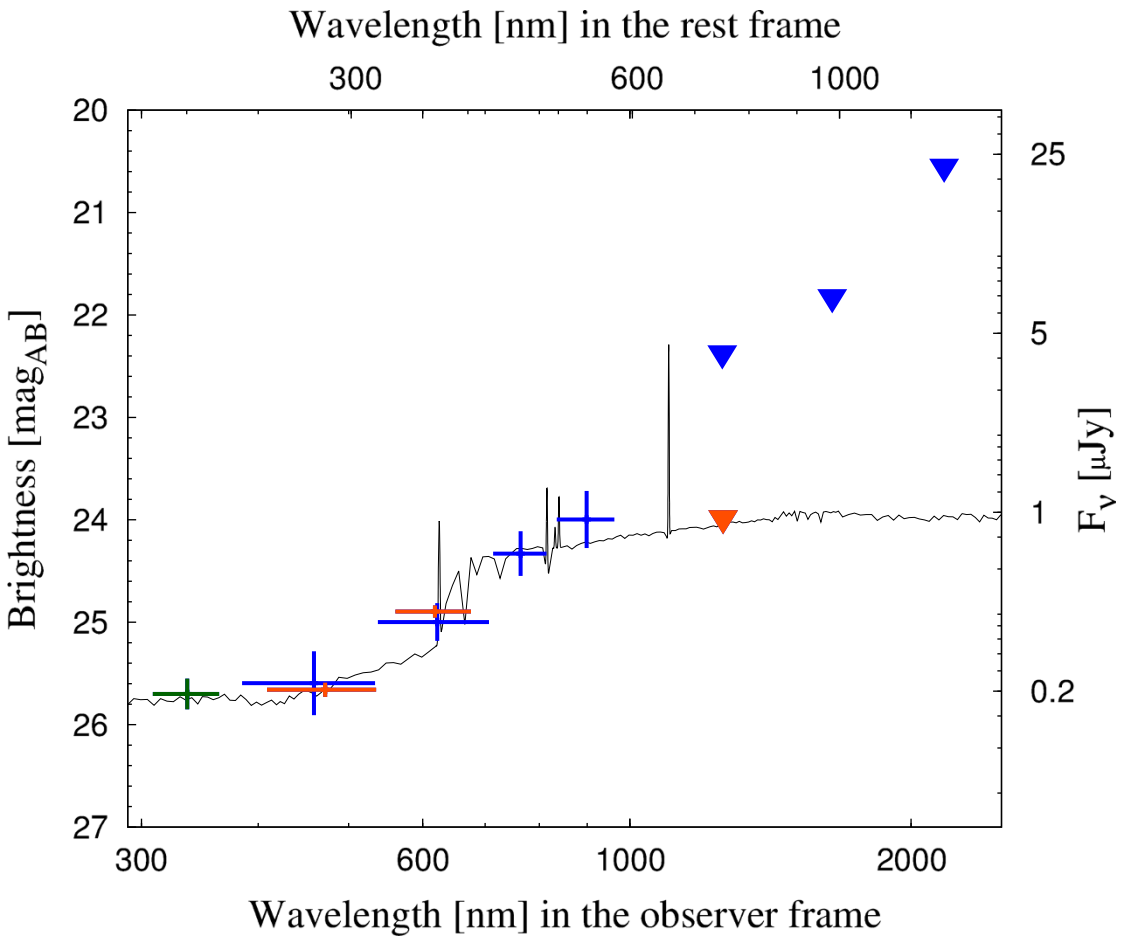

Extended Data Figure 4 | Observed spectral energy distribution of the host galaxy of GRB 111209A. Plotted in blue are GROND g′, r′, i′, z′ detections with 1σ errors (crosses) and GROND J, H, K_S upper limits (3σ; triangles) of the host galaxy of GRB 111209A. Data taken from ref. 3 are F336W (green), Gemini g′, r′ detections (red crosses) and the J-band upper limit (red triangle). The best-fit LePHARE template of a low-mass, low-extinction, young star-forming galaxy is shown, which is very typical for GRB host galaxies.

Extended Data Table 1 | GROND observations of the afterglow, supernova and host of GRB 111209A

Δt (ks)	T_{VIS} (s)	g′ (mag)	r′ (mag)	i′ (mag)	z′ (mag)	T_{NIR} (s)	J (mag)	H (mag)	K_s (mag)
151.49	460	20.05± 0.05	19.66± 0.02	19.36± 0.03	19.13± 0.02	480	18.72± 0.12	18.31± 0.12	17.84± 0.15
155.91	460	20.07± 0.06	19.62± 0.02	19.39± 0.03	19.13± 0.02	480	18.79± 0.08	18.31± 0.11	17.87± 0.15
160.33	460	20.05± 0.04	19.65± 0.02	19.36± 0.02	19.15± 0.02	480	18.75± 0.10	18.35± 0.10	18.01± 0.16
164.70	460	20.14± 0.05	19.75± 0.04	19.43± 0.03	19.19± 0.04	480	18.75± 0.11	18.40± 0.12	18.09± 0.18
239.81	919	20.81± 0.04	20.35± 0.03	20.11± 0.02	19.89± 0.05	960	19.66± 0.13	19.01± 0.14	18.71± 0.17
250.95	919	20.85± 0.06	20.49± 0.02	20.20± 0.03	19.95± 0.07	960	19.65± 0.11	19.11± 0.12	18.98± 0.21
329.17	1133	21.16± 0.06	20.74± 0.03	20.43± 0.03	20.22± 0.05	1920	19.87± 0.08	19.39± 0.12	19.10± 0.18
415.47	1838	21.49± 0.05	21.08± 0.03	20.81± 0.02	20.60± 0.04	1920	20.17± 0.11	19.88± 0.16	19.65± 0.26
501.08	1838	21.59± 0.03	21.19± 0.02	20.90± 0.02	20.71± 0.04	1920	20.25± 0.11	19.99± 0.15	19.94± 0.32
588.10	1838	21.85± 0.05	21.46± 0.03	21.18± 0.04	20.94± 0.05	1920	20.62± 0.16	20.25± 0.19	19.67± 0.27
669.18	919	22.03± 0.05	21.67± 0.08	21.40± 0.09	21.17± 0.08	960	20.70± 0.23	20.36± 0.29	19.86± 0.35
843.66	1379	22.39± 0.03	22.01± 0.03	21.75± 0.04	21.57± 0.06	1440	21.23± 0.21	20.71± 0.40	20.49± 0.46
1101.93	2420	22.86± 0.06	22.42± 0.04	22.20± 0.07	22.03± 0.09	2160	21.83± 0.24	20.82± 0.25	20.57± 0.52
1880.55	2952	23.26± 0.09	22.68± 0.05	22.40± 0.07	22.30± 0.09	2400	21.79± 0.24	21.76± 0.27	20.70± 0.75
2401.32	4502	23.45± 0.19	23.00± 0.09	22.63± 0.11	22.36± 0.14	3600	22.15± 0.32	21.86± 0.36	>20.32
3090.97	3630	23.80± 0.12	23.11± 0.08	22.81± 0.10	22.46± 0.12	3240	>22.25	>21.85	>20.22
4258.44	5384	24.27± 0.24	23.60± 0.13	23.26± 0.23	23.00± 0.32	4560	>21.54	>21.05	>19.19
4732.20	5422	24.47± 0.35	23.92± 0.15	23.38± 0.16	23.15± 0.21	4560	>22.06	>21.62	>20.33
6241.88	2758	>24.57	24.45± 0.28	23.68± 0.32	23.47± 0.44	2880	>21.52	>20.91	>20.06
24277.46	3752	25.66± 0.31	25.04± 0.18	24.36± 0.22	24.02± 0.28	3600	>22.39	>21.84	>20.56

The Δt time gives the mid-time of the observation relative to the Swift trigger time, and T_{VIS} and T_{NIR} are the exposure times in the g′r′I′z and JHK$_s$ filters, respectively. All magnitudes are in the AB system and not corrected for Galactic foreground extinction. Conversion to Vega magnitudes: $g'_{AB} - g'_{Vega} = -0.062$ mag, $r'_{AB} - r'_{Vega} = 0.178$ mag, $i'_{AB} - i'_{Vega} = 0.410$ mag, $i'_{AB} - i'_{Vega} = 0.543$ mag, $J_{AB} - J_{Vega} = 0.929$ mag, $H_{AB} - H_{Vega} = 1.394$ mag, $K_{S,AB} - K_{S,Vega} = 1.859$ mag. Corrections for Galactic extinction are $A_{g'} = 0.066$ mag, $A_{r'} = 0.046$ mag, $A_{i'} = 0.034$ mag, $A_{z'} = 0.025$ mag, $A_J = 0.015$ mag, $A_H = 0.010$ mag, $A_{K_s} = 0.006$ mag.

Extended Data Table 2 | UVOT observations of the afterglow of GRB 111209A

Δ t (ks)	T (s)	u (mag)
139.3566	546.0	$20.23^{+0.11}_{-0.10}$
187.4401	157.0	$21.14^{+0.77}_{-0.45}$
199.3795	157.0	$21.24^{+0.58}_{-0.38}$
211.8172	157.0	$21.72^{+0.77}_{-0.45}$
223.9091	235.5	$21.25^{+0.42}_{-0.30}$
233.6637	235.5	$21.75^{+0.90}_{-0.49}$
245.1895	156.9	$20.82^{+0.55}_{-0.36}$
256.7393	157.0	$21.74^{+2.17}_{-0.68}$
286.4793	84.7	>20.66
315.6230	314.1	$21.84^{+0.70}_{-0.42}$
332.6649	382.4	$21.98^{+0.52}_{-0.35}$
357.8214	844.0	$21.78^{+0.51}_{-0.34}$
428.4023	578.3	$22.05^{+0.44}_{-0.31}$
465.3887	342.0	$21.45^{+0.42}_{-0.30}$

The Δt time gives the mid-time of the observation relative to the Swift trigger time, and all magnitudes are in the AB system and not corrected for Galactic foreground extinction. Conversion to Vega magnitudes: $u_{AB} - u_{Vega} = 1.02$ mag (as given at http://swift.gsfc.nasa.gov/analysis/uvot_digest/zeropts.html). The correction for Galactic extinction, using $E_{(B-V)} = 0.017$ mag[36] and the Galactic extinction curve[46] is $A_u = 0.085$ mag.